

Supplementary Materials

Copper-doped TiO₂ photocatalyst for advanced oxidation processes: reactive oxygen species generation mechanisms

Naizhen Yu^{1,2}, Collins Nganou², Dongchang Yang², Andrew Carrier², Ken Oakes³, Mita Dasog^{1,*}, Xu Zhang^{2,*}

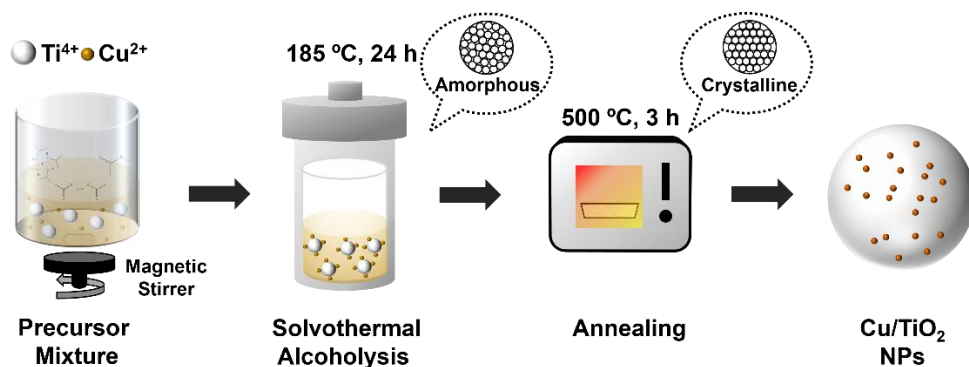
¹Department of Chemistry, Dalhousie University, Halifax B3H 4R2, Nova Scotia, Canada.

²Department of Chemistry, Cape Breton University, Sydney B1P 6L2, Nova Scotia, Canada.

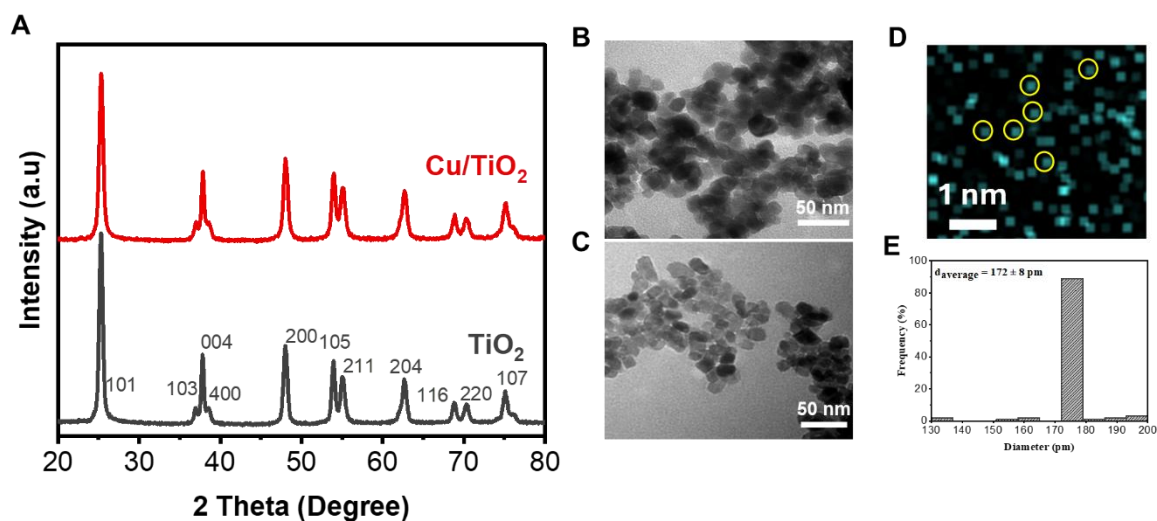
³Department of Biology, Cape Breton University, Sydney B1P 6L2, Nova Scotia, Canada.

***Correspondence to:** Prof. Mita Dasog, Department of Chemistry, Dalhousie University, 6299 South St., Halifax B3H 4R2, Nova Scotia, Canada. E-mail: mita.dasog@dal.ca; Prof. Xu Zhang, Department of Chemistry, Cape Breton University, 1250 Grand Lake Rd., Sydney B1P 6L2, Nova Scotia, Canada. E-mail: xu_zhang@cbu.ca

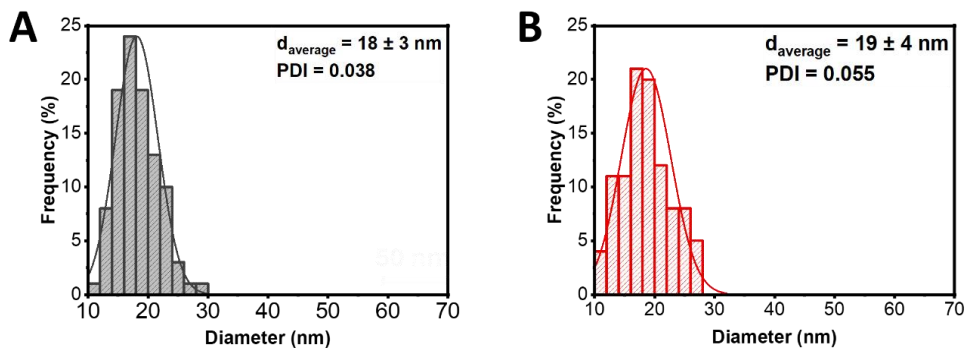
Supplementary Figures



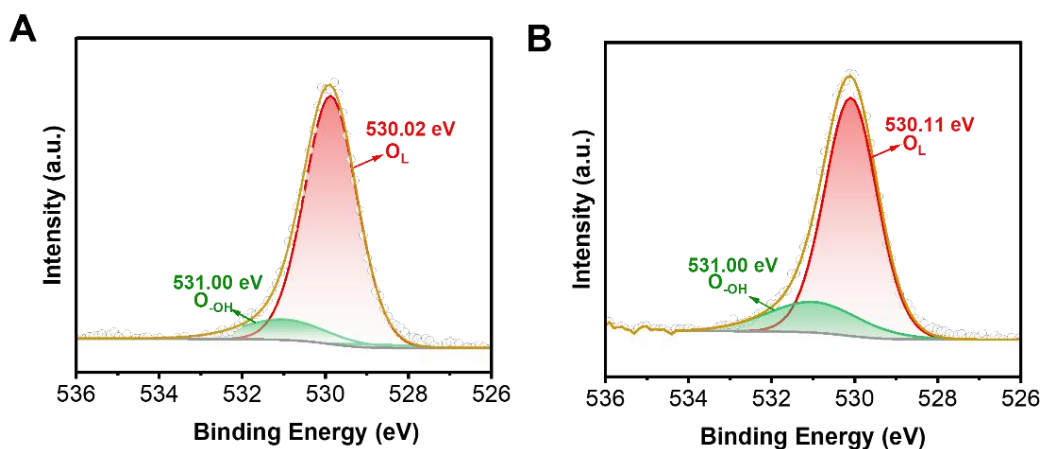
Supplementary Figure 1. Synthesis of Cu/TiO₂ nanocatalyst via solvothelmal alcoholysis.



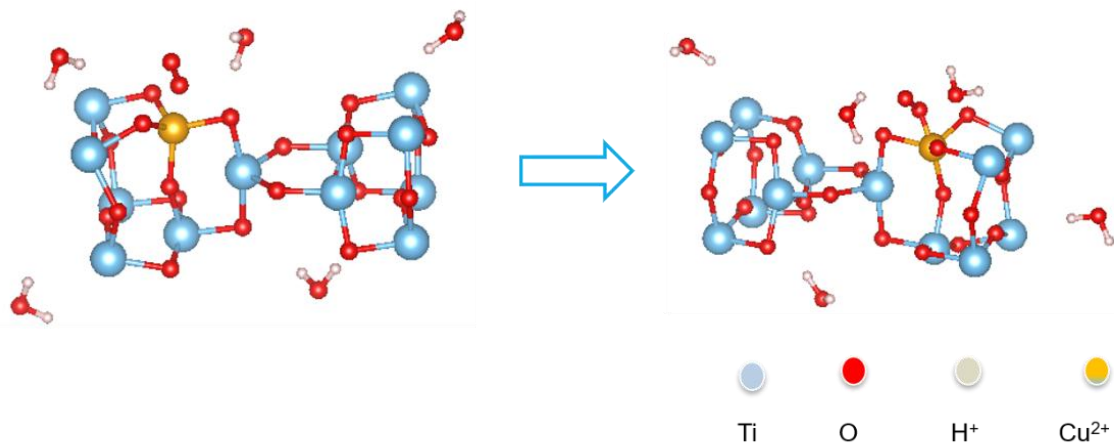
Supplementary Figure 2. (A) The XRD patterns of TiO₂ and Cu/TiO₂. TEM images of (B) TiO₂ and (C) Cu/TiO₂. The EDX-based Cu image (D) showing the size of discrete Cu atoms within Cu/TiO₂ catalyst being ~ 172 ± 8 pm (E).



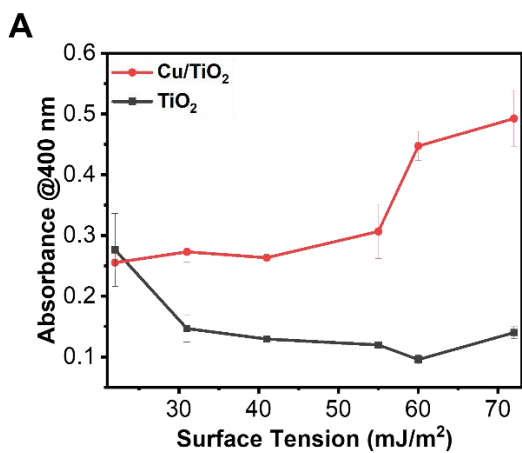
Supplementary Figure 3. The size distribution of (A) TiO₂ and (B) Cu/TiO₂ nanoparticles.



Supplementary Figure 4. High-resolution XPS spectra: The O 1s region for (A) TiO₂ and (B) Cu/TiO₂. O_L: Lattice oxygen. O_{-OH}: Surface adsorbed oxygen.



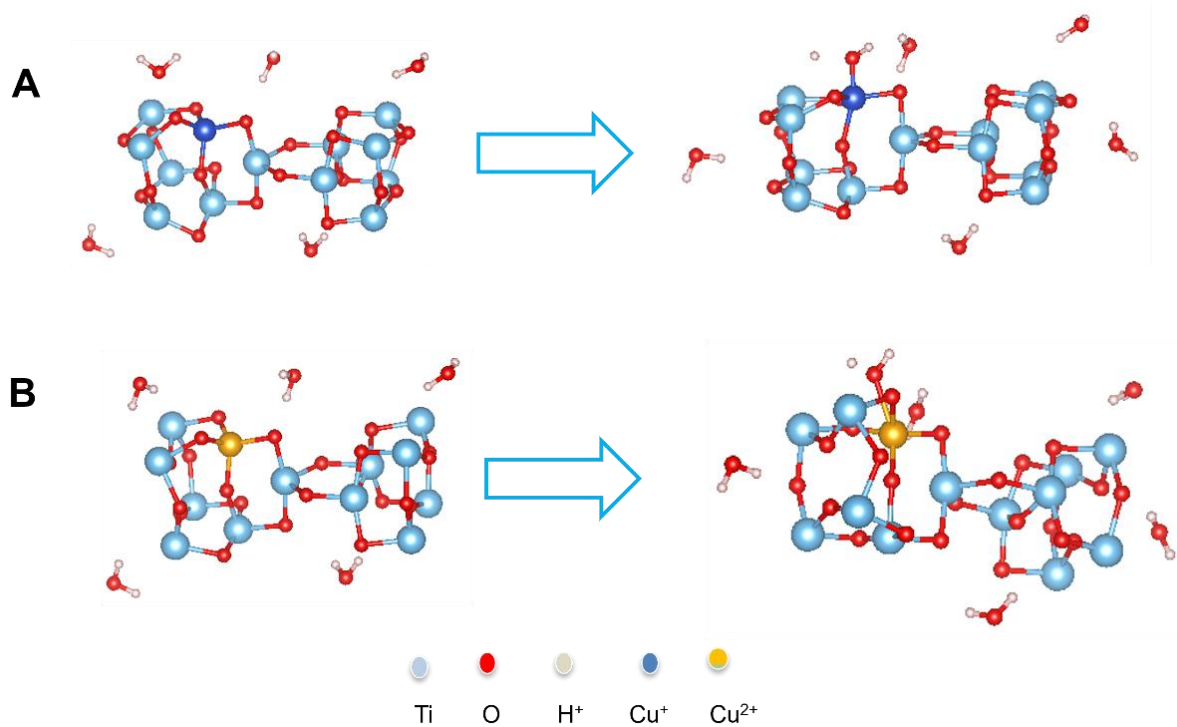
Supplementary Figure 5. The computational simulation of the adsorption (physisorption) of dissolved oxygen on the Cu/TiO₂ surfaces in water.



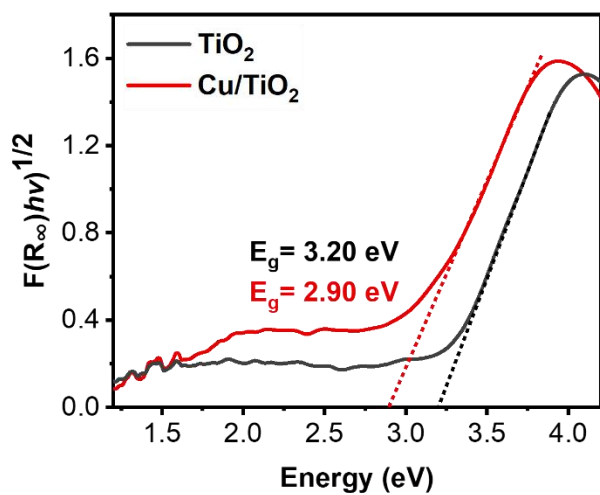
B

Volumetric Percentage of Ethanol	Surface Tension (mJ/m ²)
0%	72
5%	60
10%	55
20%	41
40%	31
100%	22

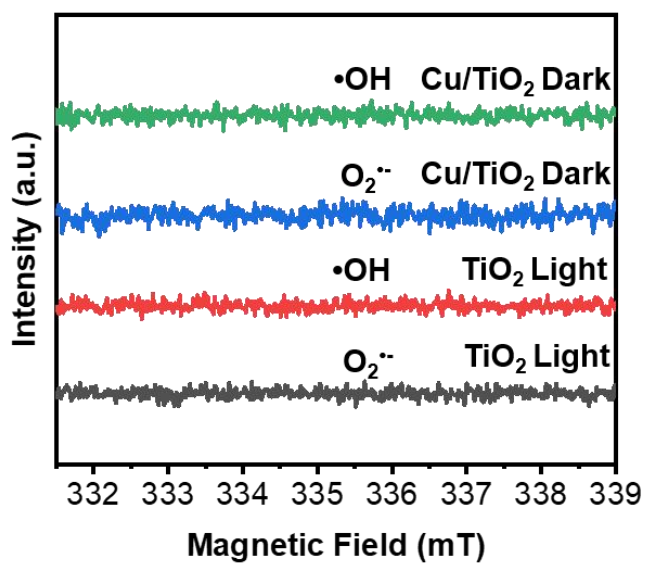
Supplementary Figure 6. Hydrophilicity analysis. (A) Particle absorbance relative to solution surface tension for TiO₂ and Cu/TiO₂ nanoparticles. (B) Surface tensions of different volumetric percentage of ethanol solutions as probing liquids.



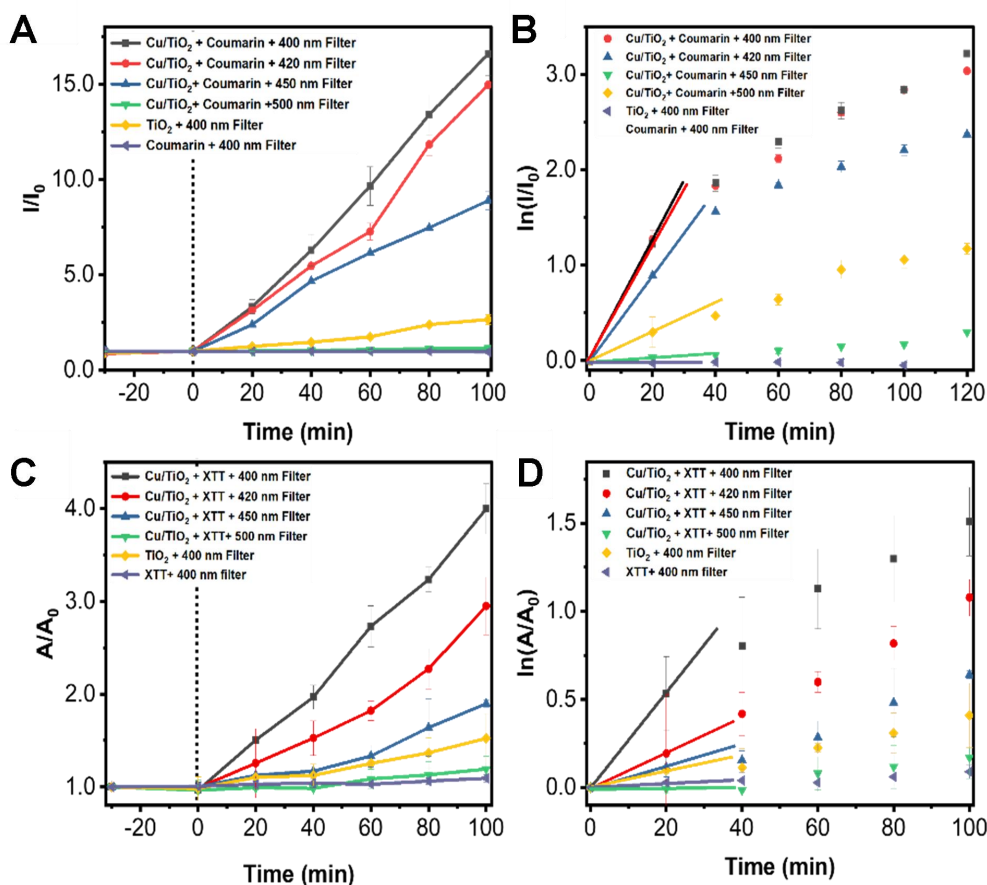
Supplementary Figure 7. The computational simulation of the adsorption (physisorption) of water on the Cu/TiO₂ surfaces through both (A) Cu⁺ (excited state) and (B) Cu²⁺ (ground state).



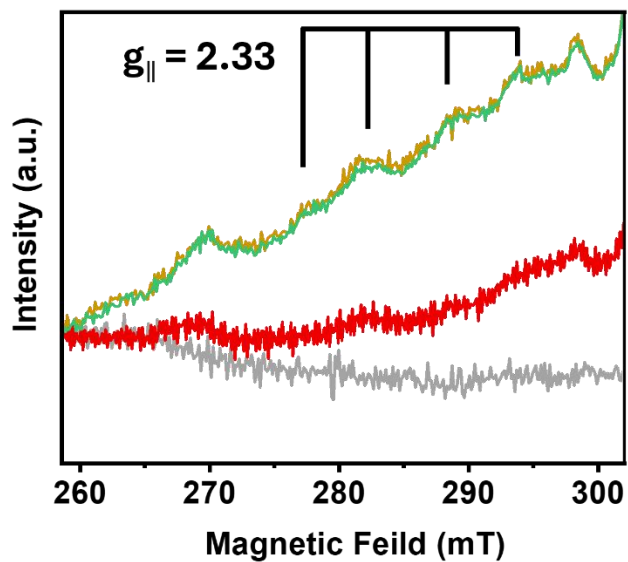
Supplementary Figure 8. Tauc plots for TiO_2 and Cu/TiO_2 .



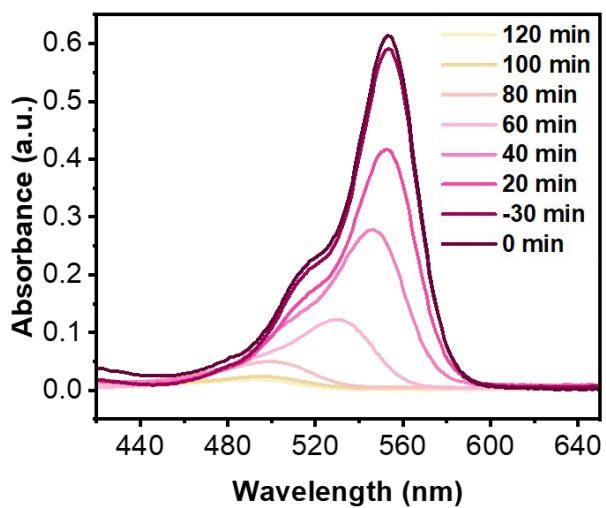
Supplementary Figure 9. The EPR spectra of radical adducts trapped by DMPO in TiO_2 under visible light, and Cu/TiO_2 samples under dark environment.



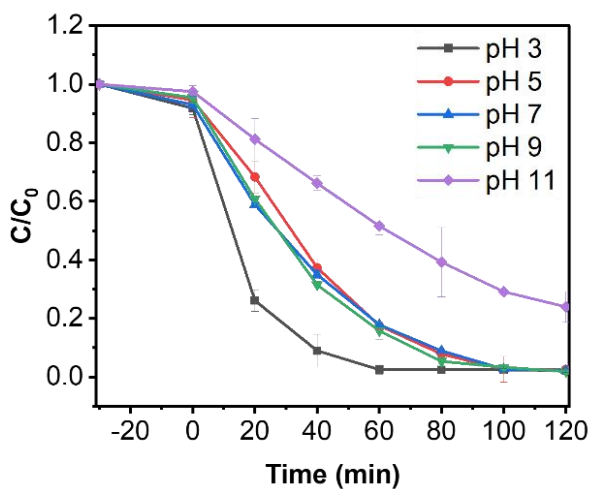
Supplementary Figure 10. ROS production kinetics by Cu/TiO₂ nanoparticles under visible light irradiation at various wavelengths. (A) $\cdot\text{OH}$ production was measured with coumarin as the probe and (B) first-order fitting to determine the initial rates. (C) $\text{O}_2^{\cdot-}$ production was measured with XTT as the probe and (D) first-order fitting to determine its initial rates.



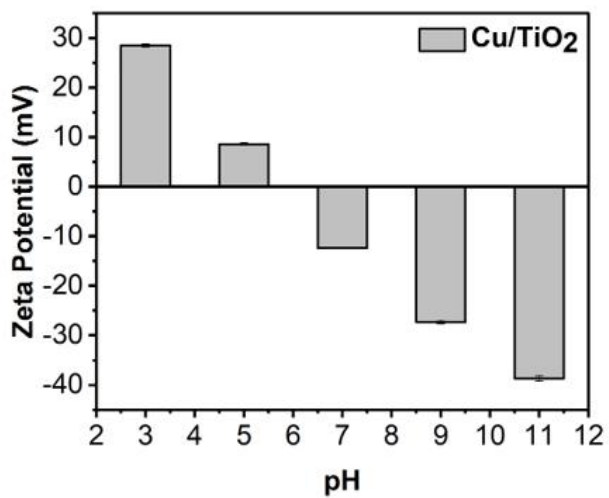
Supplementary Figure 11. The characteristic hyperfine structure of the Cu^{2+} signal under nitrogen.



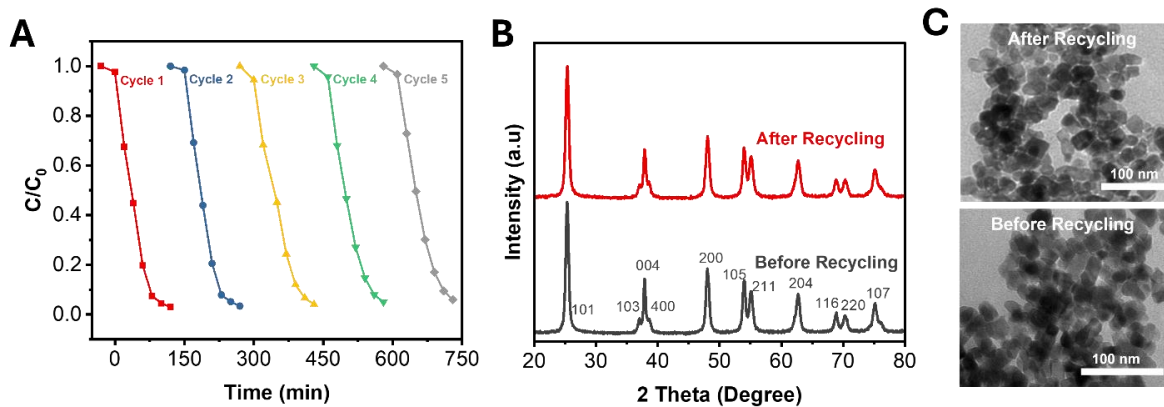
Supplementary Figure 12. The UV-vis absorption spectra of aqueous RhB solution containing Cu/TiO_2 under visible light irradiation over time.



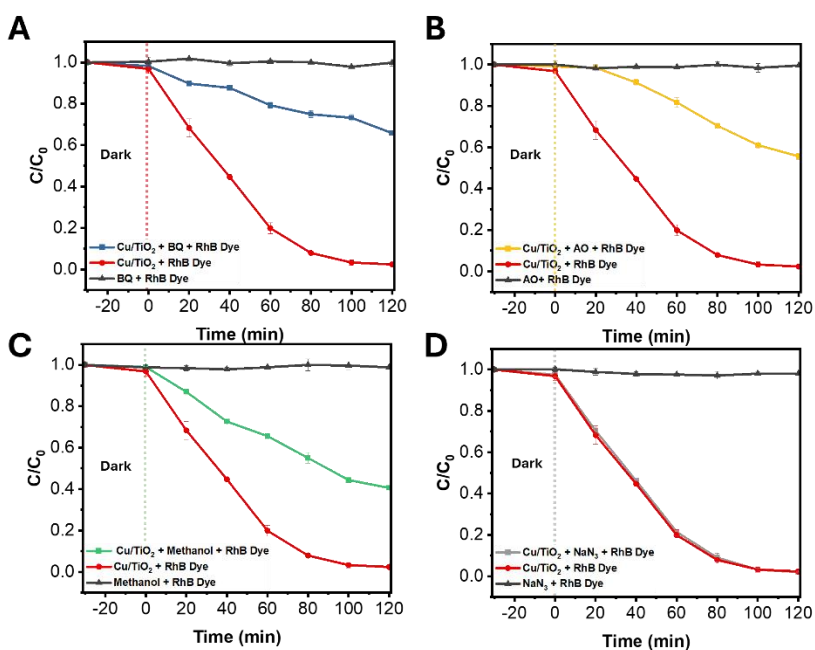
Supplementary Figure 13 Influence of pH on the degradation of rhodamine B using the Cu/TiO₂ photocatalyst.



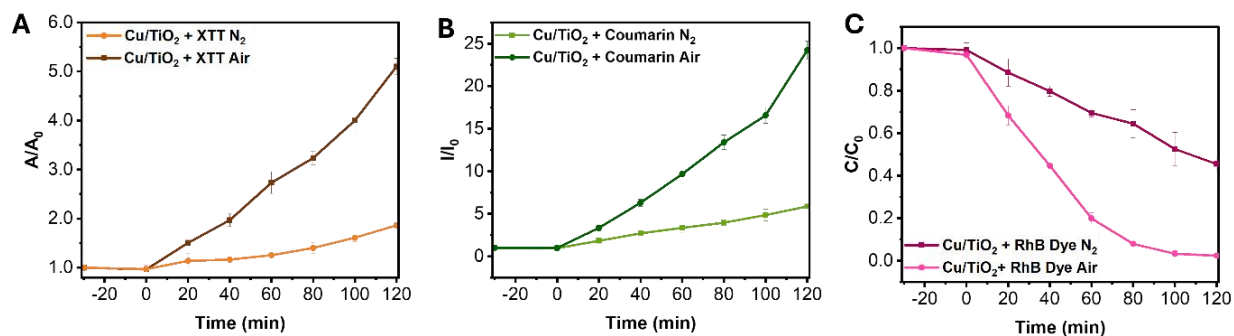
Supplementary Figure 14 Influence of pH on zeta potential of the Cu/TiO₂ photocatalyst.



Supplementary Figure 15. (A) Recyclability of Cu/TiO₂ for photocatalytic degradation of Rhodamine B over five cycles. (B) Powder XRD patterns and (C) TEM images of Cu/TiO₂ before and after recycling.



Supplementary Figure 16. The photodegradation of RhB by Cu/TiO₂ catalysts under visible light irradiation in the presence of four scavengers: (A) 1,4-Benzoquinone (BQ), (B) ammonium oxalate (AO), (C) methanol, and (D) sodium azide (NaN₃).



Supplementary Figure 17. The formation of (A) $O_2^{\cdot-}$ probed by XTT and (B) $\cdot OH$ probed by coumarin using Cu/TiO₂ nanocatalysts under N₂ or air with visible light irradiation. (C) The photodegradation of RhB by Cu/TiO₂ nanocatalysts under N₂ or air with visible light irradiation.

Cu/TiO₂ + *E. coli* under Irradiation



Cu/TiO₂ + *E. coli* in the Dark



TiO₂ + *E. coli* under Irradiation

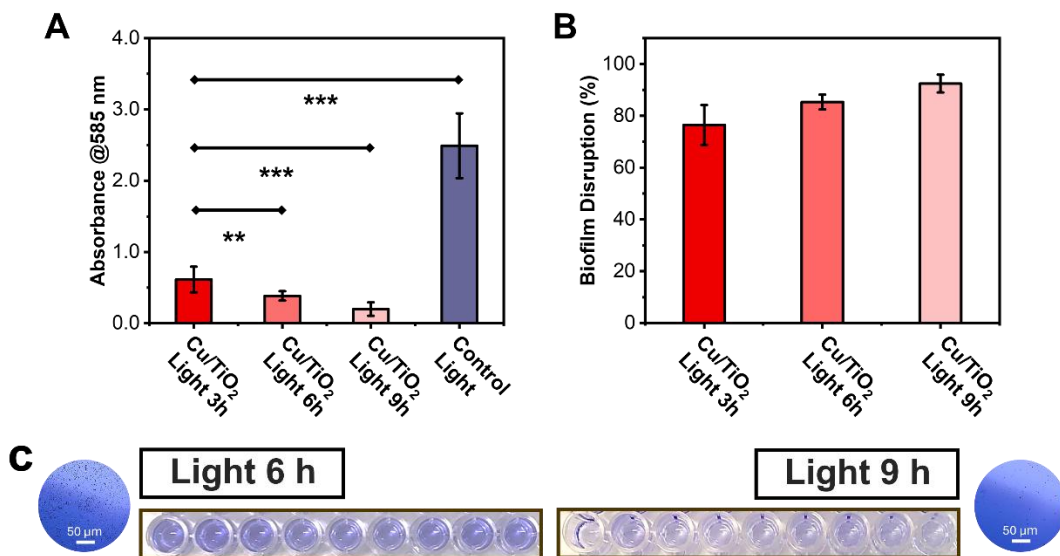


TiO₂ + *E. coli* in the Dark



0 20 40 60 80 100 120 140 160 180 (min)

Supplementary Figure 18. The bactericidal efficiency of Cu/TiO₂ and undoped TiO₂ nanoparticles with and without visible light irradiation.



Supplementary Figure 19. (A) The biofilm disruption efficiency of Cu/TiO₂ NPs under visible light irradiation for 3-9 hours assayed by using crystal violet dye. (B) The calculated biofilm disruption percentages. (C) the Optical and microscopic images of the biofilm in the microplate wells after treatment (n = 9).

Supplementary Tables

Supplementary Table 1. Elemental analysis of Cu/TiO₂ via energy-dispersive X-ray (EDX) spectroscopy

Atomic Number	Element	Atomic fraction (%)	Mass Fraction (%)	Fit Error (%)
8	O	67.82 ± 3.69	41.29 ± 4.09	1.75
22	Ti	32.02 ± 3.7	58.33 ± 4.13	0.21
29	Cu	0.16 ± 0.02	0.38 ± 0.07	0.50

Supplementary Table 2. Comparison of photoelectrical properties of various Cu/TiO₂ samples

Materials	[Cu] ₀ (mM)	Light Intensity (mW/cm ²)	Light Wavelength (nm)	Light Source	Photocurrent Intensity (uA/cm ²)	Charge Transfer Resistance (ohm)	Band Gap (eV)	Application	Reference
Cu-doped TiO ₂ NPs	0.08	3	UV	Flashlight	2.5	>16	2.69	Rewritable Printing	[1]
Cu Surface doped TiO ₂	2.23	N/A	UV+Visible Light	300 W Xenon Lamp	1.6	N/A	2.95	Hydrogen Production	[2]
Cu-doped TiO ₂ NPs	18.55	100	>400 (with blocking filter)	500 W Xenon Lamp	55	N/A	2.3	Dye Degradation	[3]
Cu-doped TiO ₂ NPs	10	100	>400 (with blocking filter)	150 W Xenon Lamp	0.25	N/A	2.96	Viral Inactivation	[4]
Cu-doped TiO ₂	165.7	100	UV+Visible Light	UV+Visible LED Lights	0.1	192	2.7	Hydrogen Evolution	[5]

Cu-doped TiO ₂ Thin Film	N/A	0.00528	315-400 and 450-950	5 W LED Light	30	0.61	N/A	Photoelectrochemical Cells	[6]
Cu-doped TiO ₂ NPs	0.55	100	400-800	100 W Visible LED Light	3	6	2.9	Dye Degradation and Killing Bacteria	Current Work

NPs: Nanoparticles, [Cu]₀: Cu initial concentration; UV: Ultraviolet; LED: Light-emitting diode; N/A: Not Applicable

Supplementary Table 3. ROS generation kinetics (A) $\cdot\text{OH}$ and (B) $\text{O}_2^{\cdot-}$ production under visible light irradiation at various wavelengths. The reaction rate was calculated based on the first 40-minute results

A

Sample	Kinetic Equation	R²
Cu/TiO ₂ + Coumarin + 400 nm Filter	$y = 0.1322x + 0.8954$	0.99
Cu/TiO ₂ + Coumarin + 420 nm Filter	$y = 0.1117x + 0.9677$	0.99
Cu/TiO ₂ + Coumarin + 450 nm Filter	$y = 0.0917x + 0.8521$	0.98
Cu/TiO ₂ + Coumarin + 500 nm Filter	$y = 0.0009x + 0.9962$	0.89
TiO ₂ + Coumarin + 400 nm Filter	$y = 0.0118x + 1.0038$	0.99
Coumarin + 400 nm Filter	$y = -0.00013x$	0.85

B

Sample	Kinetic Equation	R²
Cu/TiO ₂ + XTT + 400 nm Filter	$y = 0.0251x + 0.9785$	0.99
Cu/TiO ₂ + XTT + 420 nm Filter	$y = 0.0134x + 0.9911$	0.99
Cu/TiO ₂ + XTT + 450 nm Filter	$y = 0.0042x + 1.0143$	0.93
Cu/TiO ₂ + XTT + 500 nm Filter	$y = 0.0005x + 0.9711$	0.81
TiO ₂ + XTT + 400 nm Filter	$y = 0.0035x + 1.0011$	0.86
XTT + 400 nm Filter	$y = 0.0009x + 1.0088$	0.97

Supplementary Table 4. Comparison of photodegradation, antibacterial, and antibiofilm efficiency of various Cu/TiO₂ samples

Research	Materials	[Cu] ₀ (mM)	[Pollutant] Pollutant (ppm or CFU/mL)	Light Source	Light Intensity (mW/cm ²)	Wavelength (nm)	Treatment Time (Hours)	Pseudo 1 st -order		Reference
								Rate Constant (min ⁻¹)		
Photodegradation Efficiency	Cu-doped Mesoporous TiO ₂ NPs	92.08	Methyl Orange	50	50 W Xenon Lamp	N/A	220-1000	1.67	-	[7]
	Cu - Doped TiO ₂ NPs	200	RhB	5	5000 W LED	100	350-800	2	0.0147	[8]
	Cu-doped mesoporous TiO ₂	100	Congo Red	8	Mercury Lamp	5800	N/A	1.67	0.0505	[9]
	Cu-doped TiO ₂ NPs	0.55	RhB	5	100 W LED	100	400-800	1.67	0.0341	Current Work
Bacterial Killing Efficiency	Cu-Doped TiO ₂ NPs	N/A	<i>MRSA</i>	4×10 ⁸	250 W Xenophot bulb	65-85	400-700 (with UV filter)	1.5	N/A	[10]
	Cu-doped TiO ₂ NPs	4.8	<i>E. coli</i>	1.7×10 ⁴	300 W Xenon Lamp	100	> 400 (with UV filter)	24	N/A	[11]

	Cu-Doped TiO ₂ Thin Films	35	<i>E. coli and S. aureus</i>	1.0×10 ⁵	16 W UVA Lamp	3.15	345-405	4	N/A	[12]
	Cu-doped TiO ₂ NPs	0.55	<i>E. coli</i>	1.0×10 ⁶	100 W Visible LED	100	400-800	1.67	N/A	Current Work
Biofilm Degradation Efficiency	CuO@TiO ₂ Nanocomposites	3	<i>P. aeruginosa</i> + <i>MRSA</i>	N/A	N/A	N/A	N/A	24	N/A	[13]
	Cu-doped TiO ₂ NPs	0.55	<i>E. coli</i>	N/A	100 W Visible LED	100	400-800	9	N/A	Current Work

NPs: Nanoparticles; *MRSA*: *Methicillin-resistant Staphylococcus aureus*; RhB: rhodamine B; UV: Ultraviolet; LED: light-emitting diode; N/A: Not Applicable.

References:

1. Wang, W., Wei, D., Zhang, Y., Ye, Y., Dou, Y., Guo, J., ... & Yin, Y. Photoreversible color-switching Cu-doped TiO₂ nanoparticles for high-contrast rewritable printing. *ACS Nano* 2024, DOI: 10.1021/acsnano.4c11212.
2. Xiao, B., Shen, C., Luo, Z., Li, D., Kuang, X., Wang, D., ... & Liu, Q. Cu surface-doped TiO₂: Constructing Cu single-atoms active sites and broadening the photo-response range for efficient photocatalytic hydrogen production. *Chem. Eng. J.* 2023, 468, 143650, DOI: 10.1016/j.cej.2023.143650.
3. Reda, S. M., Khairy, M., & Mousa, M. A. Photocatalytic activity of nitrogen and copper-doped TiO₂ nanoparticles prepared by microwave-assisted sol-gel process. *Arab. J. Chem.* 2020, 13(1), 86-95, DOI: 10.1016/j.arabjc.2017.02.002.
4. Kim, J., Lee, J., Kim, S., Kim, T., Lee, K. M., Lee, D., ... & Lee, C. Virucidal activity of Cu-doped TiO₂ nanoparticles under visible light illumination: Effect of Cu oxidation state. *J. Hazard. Mater.* 2024, 465, 133525, DOI: 10.1016/j.jhazmat.2024.133525.
5. Xing, C., Zhang, Z., Zhang, Y., Han, X., Yang, L., Li, J., ... & Cabot, A. Synergistic effect of surface oxygen vacancies and hydroxyl groups on Cu-doped TiO₂ photocatalyst for hydrogen evolution. *Mater. Today Nano* 2023, 24, 100435, DOI: 10.1016/j.mtnano.2023.100435.
6. Garlisi, C., Lai, C. Y., George, L., Chiesa, M., & Palmisano, G. Relating photoelectrochemistry and wettability of sputtered Cu- and N-doped TiO₂ thin films via an integrated approach. *J. Phys. Chem. C* 2018, 122(23), 12369-12376, DOI: 10.1021/acs.jpcc.8b03650.
7. Wang, Y., Duan, W., Liu, B., Chen, X., Yang, F., & Guo, J. The effects of doping copper and mesoporous structure on photocatalytic properties of TiO₂. *J. Nanomater.* 2014, 2014(1), 178152, DOI: 10.1155/2014/178152

8. Raguram, T., & Rajni, K. S. Synthesis and characterisation of Cu-doped TiO₂ nanoparticles for DSSC and photocatalytic applications. *Int. J. Hydrogen Energy* 2022, 47(7), 4674-4689, DOI: 10.1016/j.ijhydene.2021.11.113.
9. Bibi, S., Shah, S. S., Muhammad, F., Siddiq, M., Kiran, L., Aldossari, S. A., ... & Sarwar, S. Cu-doped mesoporous TiO₂ photocatalyst for efficient degradation of organic dye via visible light photocatalysis. *Chemosphere* 2023, 339, 139583, DOI: 10.1016/j.chemosphere.2023.139583.
10. Campbell, Z. S., Ghareeb, C. R., Baro, S., Mauthe, J., McColgan, G., Amassian, A., ... & Dickey, E. C. Facile synthesis of Cu-doped TiO₂ particles for accelerated visible light-driven antiviral and antibacterial inactivation. *ACS Appl. Eng. Mater.* 2024, 2(5), 1411-1423, DOI: 10.1021/acsaenm.4c00176.
11. Wang, F., Yang, S., Lu, Q., Liu, W., Sun, P., Wang, Q., & Cao, W. Colloidal Cu-doped TiO₂ nanocrystals containing oxygen vacancies for highly efficient photocatalytic degradation of benzene and antibacterial. *Colloids Surf., A* 2023, 658, 130741, DOI: 10.1016/j.colsurfa.2022.130741.
12. Alotaibi, A. M., Williamson, B. A., Sathasivam, S., Kafizas, A., Alqahtani, M., Sotelo-Vazquez, C., ... & Parkin, I. P. Enhanced photocatalytic and antibacterial ability of Cu-doped anatase TiO₂ thin films: theory and experiment. *ACS Appl. Mater. Interfaces* 2020, 12(13), 15348-15361, DOI: 10.1021/acsaami.9b22056.
13. Baig, U., Ansari, M. A., Gondal, M. A., Akhtar, S., Khan, F. A., & Falath, W. S. Single-step production of high-purity copper oxide-titanium dioxide nanocomposites and their effective antibacterial and anti-biofilm activity against drug-resistant bacteria. *Mater. Sci. Eng., C* 2020, 113, 110992, DOI: 10.1016/j.msec.2020.110992.